Complex Angular Momentum Methods in the Study of Nucleon-Nucleus Elastic Scattering

R. Shanta
Saha Institute of Nuclear Physics, Calcutta,
and Nuclear Physics Division, Bhabha Atomic Research Centre, Bombay, India
and
R. K. Satpathy
Department of Physics, Ravenshaw College, Cuttack, India
(Received 22 October 1969; revised manuscript received 27 March 1970)

The complex angular momentum technique is applied to the study of nucleon-nucleus elastic scattering. Regge-type representations are developed for the scattering amplitude, taking the spin of the incident nucleon into account. The pole parameters are determined using the optical-potential parameters as input. With these pole parameters, the differential cross sections for elastic nucleon-nucleus scattering are calculated using an appropriate Regge-type representation for the partial-wave amplitudes. These studies give insight into the applicability of complex angular momentum methods to the optical model of elastic scattering of nucleons from nuclei.

I. INTRODUCTION

Recently the Regge-pole theory[1] has found much application in the analysis of nuclear scattering and reactions.[2-5] The analytical properties of the S matrix or partial-wave amplitude in the complex λ $(=l+\frac{1}{2})$ plane are utilized for the investigation of these problems. It has been shown[6] that it is possible, in principle, to formulate Regge-type representations for the partial-wave amplitudes such that they not only exhibit the correct physical features of the S matrix, namely, correct threshold behavior in momentum, asymptotic behavior in angular momentum, and unitarity, but can also make the effect of the background integral small. Representations of this type for the S matrix, having all the necessary physical features and small background effects, have been used in the analysis of elastic scattering of α particles by spinless charged target nuclei.[4]

Most of the earlier works[2-4] on the application of complex angular-momentum methods to nuclear scattering deal with the analysis of elastic scattering of spinless charged particles. In a recent work,[5] the effect of spin-orbit interaction has been investigated. It has been shown, by considering a complex optical potential with a spin-orbit part, that the Regge poles corresponding to the physical states of the interacting system appear not only along the positive real axis and the upper right half of the λ plane, but also in the fourth quadrant of the complex λ plane.

In the present paper, we consider the scattering of protons and neutrons from spinless charged target nuclei such as C^{12}, O^{16}, and Ca^{40}. Here we take into account the spin of the incident particles in deriving the Regge-type representations. Usually the optical potential is quite successful in reproducing the experimental scattering data for heavy- and medium-weight nuclei. So for most cases for which experimental phase-shift data are not available, the optical potential is utilized for obtaining the pole parameters for a given nucleon-nucleus scattering. These pole parameters together with an appropriate Regge-type representation for the S matrix are used for calculating the differential cross sections. This analysis helps us to investigate the validity of the Regge-pole approach to the optical model of elastic scattering of nucleons from nuclei.

II. COMPLEX OPTICAL POTENTIAL

It is known that the complex optical potential is quite capable of explaining the experimental scattering data for medium-weight nuclei. The elastic scattering depends essentially on both the real and imaginary parts of the potential. The imaginary part of the optical potential takes care of the absorption processes which include all inelastic processes. When we consider the scattering of nucleons from nuclei, it is observed that the scattered particles are polarized. This can be explained by an optical potential only if it contains a spin-dependent part. The generalized optical potential may be written as

$$V_{\text{opt}}(r) = -U_n v(r) - iW_n f_1(r) + (U_s + iW_s)(\hbar/m_\pi c)^2 f_2(r)\vec{l}\cdot\vec{\sigma}, \tag{2.1}$$

where

$$v(r) = [1 + e^{(r - r_0/a_0)}]^{-1} \tag{2.2}$$

is the radial variation of the real part, and U_n the

corresponding strength; $f_1(r)$ is the radial variation of the imaginary part, and W_n the corresponding strength of the potential. U_s and W_s are the real and imaginary parts of the spin-dependent potential, $f_2(r)$ is their radial variation, σ is the Pauli spin operator, r_0 the radius of the nucleus, and a_0 the corresponding diffuseness parameter.

The spin of the incident particle can couple in two ways to the orbital angular momentum l to give the total angular momentum $j = l \pm \frac{1}{2}$, and the eigenvalues of $\vec{l} \cdot \vec{\sigma}$ corresponding to these two spin orientations are l and $-(l+1)$.

In this case, the S matrix not only depends upon the momentum k, and the angular momentum λ but also on the complex strength V_0 of the optical potential and hence is denoted by $S(\lambda, k, V_0)$. The unitarity relation obeyed by the S matrix $S(\lambda, k, V_0)$ is given by[5]

$$S(\lambda, k, V_0) S^*(\lambda^*, k^*, V_0^*) = 1 . \tag{2.3}$$

III. REGGE-TYPE REPRESENTATIONS FOR CHARGED-PARTICLE PARTIAL-WAVE AMPLITUDES WHEN A SPIN-ORBIT FORCE IS PRESENT

The elastic scattering of nucleons from spin-zero nuclei is conveniently described[7] in terms of the two amplitudes $A_1(k, \cos\theta)$ and $A_2(k, \cos\theta)$ where

$$A_1(k, \cos\theta) = (1/2k)[-\eta \csc^2 \tfrac{1}{2}\theta \exp(2i\sigma_0 - 2i\eta \ln \sin \tfrac{1}{2}\theta) + i \sum_{l,j} (j + \tfrac{1}{2}) e^{2i\sigma_0} (e^{2i\omega_l} - U_l) P_l(\cos\theta)] \tag{3.1}$$

and

$$A_2(k, \cos\theta) = \frac{i}{2k} \sum_{l,j} (-1)^{j-l-\frac{1}{2}} e^{2i\sigma_0} (e^{2i\omega_l} - U_l) P_l^1(\cos\theta), \tag{3.2}$$

in which

$$\omega_l = (\sigma_l - \sigma_0) = \sum_{m=1}^{l} \tan^{-1}(\eta/m),$$

σ_l is the Coulomb phase shift for the lth partial wave, k is the wave number, and η is the usual Coulomb parameter, while U_l is the collision matrix defined by Lane and Thomas.[8] U_l is given by

$$U_l = e^{-2i\sigma_0} S_l(k) = e^{2i(\sigma_l - \sigma_0)} \bar{S}_l(k) , \tag{3.3}$$

where S_l is the full S matrix, $\bar{S}_l$ is the nuclear S matrix. From the above equations we obtain

$$A_1(k, \cos\theta) = -\frac{\eta}{2k} \csc^2 \tfrac{1}{2}\theta \exp(2i\sigma_0 - 2i\eta \ln \sin \tfrac{1}{2}\theta) + \sum_l e^{2i\sigma_l} [(l+1) a^+(l,k) - l a^-(l,k)] P_l(\cos\theta) \tag{3.4}$$

and

$$A_2(k, \cos\theta) = \sum_l e^{2i\sigma_l} [a^+(l,k) - a^-(l,k)] P_l^1(\cos\theta) , \tag{3.5}$$

where $a^\pm(l,k) = [\bar{S}_l^\pm(k) - 1]/2ik$, corresponding to the total angular momentum $j = l \pm \frac{1}{2}$.

The Regge, Khuri, and modified Regge representations of Ref. 6 may be easily obtained for the partial-wave amplitudes $a^\pm(\lambda, k)$ as shown in the Appendix. We find that the Regge representation for the partial-wave amplitudes is given by

$$\frac{(\lambda \pm \frac{1}{2})^2}{2\lambda} a^\pm(\lambda, k) = \sum_{n=1}^{N^\pm} \beta_n^\pm \frac{(\lambda_n^\pm \pm \frac{1}{2})^2}{\lambda^2 - (\lambda_n^\pm)^2} , \tag{3.6}$$

where the symbols $\lambda_n^\pm$ and $\beta_n^\pm$ denote the pole positions and residues of $a^\pm(\lambda, k)$ in the right half of the λ plane, and $N^\pm$ denotes the number of poles of $a^\pm(\lambda, k)$ in this domain. λ takes half-integral values.

For the Khuri representation we obtain

$$\frac{1}{\lambda^2} a^\pm(\lambda, k) = \sum_{n=1}^{N^\pm} \beta_n^\pm \frac{1}{(\lambda_n^\pm)^2} \frac{e^{(\lambda_n^\pm - \lambda)\xi}}{\lambda - \lambda_n^\pm} . \tag{3.7}$$

For the modified Regge representation of Ref. 6, we may write

$$\frac{1}{\lambda^2} a^\pm(\lambda, k) = \sum_{n=1}^{N^\pm} \beta_n^\pm \frac{1}{(\lambda_n^\pm)^2} \frac{1}{\lambda - \lambda_n^\pm} \frac{\exp(ie^{-\lambda\xi}) - 1}{\exp(ie^{-\lambda_n^\pm \xi}) - 1} \left(\frac{2\lambda}{\lambda + \lambda_n^\pm}\right)^m , \tag{3.8}$$

where m is a suitable positive integer. In our calculations we consider only the values $m = 0$ and 1.

The above representation for $a^\pm(\lambda, k)$ has correct threshold behavior in k and asymptotic behavior in λ, and the factor $[2\lambda/(\lambda + \lambda_n^\pm)]^m$ is expected to reduce the effect of the background integral. However, when we consider charged-particle scattering, for instance proton scattering, it is desirable to incorporate the Coulomb threshold factor[4,9]

$$\mathcal{C}^2_{\lambda - \frac{1}{2}} = e^{-\pi\eta} \frac{\Gamma(\lambda + \frac{1}{2} + i\eta)\Gamma(\lambda + \frac{1}{2} - i\eta)}{[\Gamma(\lambda + \frac{1}{2})]^2} . \tag{3.9}$$

It is easily seen that when we consider neutron scattering $\eta=0$, and hence $\mathcal{G}^2_{\lambda-\frac{1}{2}}=1$. The representations (3.6) to (3.8) are modified by incorporating the factor

$$\mathcal{G}^2_{\lambda-\frac{1}{2}}/\mathcal{G}^2_{\lambda_n^{\pm}-\frac{1}{2}}\,. \tag{3.10}$$

In order to bring out the asymptotic behavior of the partial-wave amplitude explicitly, we proceed as follows. The asymptotic behavior of $a^{\pm}(\lambda,k)$ for large λ along the real axis is determined by the integral[10]

$$I=\int_0^{\infty} rV(r)J^2_{\lambda}(kr)dr\,. \tag{3.11}$$

Using the Woods-Saxon form (2.2) for $V(r)$ and using the method of Ref. 4, we obtain for large λ

$$I=(e^{-\lambda/ka_0}+e^{-r/a_0})^{-1}O(|\lambda|^{1/2}e^{-\lambda\bar{\xi}}), \tag{3.12}$$

where

$$\bar{\xi}=\cosh^{-1}(1+1/2a_0^2k^2)\,. \tag{3.13}$$

In Eq. (3.12) it must be noted that $\lambda/ka_0\simeq\lambda\xi$ in the range of energies that we have considered.

We further modify the Khuri and modified Regge-type representations by incorporating the factor

$$\frac{\lambda(e^{-\lambda_n^{\pm}\xi}+e^{-r/a_0})}{\lambda_n^{\pm}(e^{-\lambda\xi}+e^{-r/a_0})}\,, \tag{3.14}$$

as in Ref. 4.

After incorporating the factor given by Eq. (3.10) in the Regge case, and both the factors given by Eqs. (3.10) and (3.14) in the case of other representations, the final form of the representations (3.6) to (3.8) are written as follows:

$$\frac{(\lambda\pm\frac{1}{2})^2}{2\lambda}a^{\pm}(\lambda,k)=\sum_{n=1}^{N^{\pm}}\beta_n^{\pm}\frac{(\lambda_n^{\pm}\pm\frac{1}{2})^2}{\lambda^2-(\lambda_n^{\pm})^2}\,\frac{\mathcal{G}^2_{\lambda-\frac{1}{2}}}{\mathcal{G}^2_{\lambda_n^{\pm}-\frac{1}{2}}}\,. \tag{3.15}$$

Let us designate this representation as R1. The second representation, given by (3.7), has the final form

$$\frac{1}{\lambda^2}a^{\pm}(\lambda,k)=\sum_{n=1}^{N^{\pm}}\beta_n^{\pm}\frac{1}{(\lambda_n^{\pm})^2}\frac{e^{(\lambda_n^{\pm}-\lambda)\xi}}{\lambda-\lambda_n^{\pm}}\times\frac{\mathcal{G}^2_{\lambda-\frac{1}{2}}}{\mathcal{G}^2_{\lambda_n^{\pm}-\frac{1}{2}}}\,\frac{\lambda}{\lambda_n^{\pm}}\,\frac{e^{-\lambda_n^{\pm}\xi}+e^{-r/a_0}}{e^{-\lambda\xi}+e^{-r/a_0}}\,. \tag{3.16}$$

We shall designate this representation as R2. Similarly, the final form of (3.8) is

$$\frac{1}{\lambda^2}a^{\pm}(\lambda,k)=\sum_{n=1}^{N^{\pm}}\beta_n^{\pm}\frac{1}{(\lambda_n^{\pm})^2}\frac{1}{\lambda-\lambda_n^{\pm}}\left(\frac{2\lambda}{\lambda+\lambda_n^{\pm}}\right)^m\times\frac{\exp(ie^{-\lambda\xi})-1}{\exp(ie^{-\lambda_n^{\pm}\xi})-1}\,\frac{\mathcal{G}^2_{\lambda-\frac{1}{2}}}{\mathcal{G}^2_{\lambda_n^{\pm}-\frac{1}{2}}}\,\frac{e^{-\lambda_n^{\pm}\xi}+e^{-r/a_0}}{e^{-\lambda\xi}+e^{-r/a_0}}\,\frac{\lambda}{\lambda_n^{\pm}}\,. \tag{3.17}$$

We shall designate the above representation for $m=0$ by R3, and for $m=1$ by R4.

In all these representations given by Eqs. (3.15) to (3.17), the left-hand sides are calculated from known data. In most cases of elastic scattering of nucleons by nuclei, optical-potential parameters which give a good fit with experiment are available. The Schrödinger equation is numerically solved by using known optical-potential parameters, and thereby the partial-wave amplitudes $a^{\pm}(\lambda,k)$ are calculated. In cases where experimental phase shifts are known, $a^{\pm}(\lambda,k)$ may be directly evaluated. The right-hand sides of these equations represent sums over poles. It is assumed that only two poles contribute significantly to the partial wave amplitude. A two-pole approximation formula for the partial-wave amplitude has four unknowns, viz., two pole parameters and correspondingly two residue parameters. So with the known input data, $a^{\pm}(\lambda,k)$ are computed for $\lambda=\frac{1}{2}$, $\frac{3}{2}$, $\frac{5}{2}$, and $\frac{7}{2}$, thus giving four equations. These four equations are now solved to obtain the poles and residues. With this set of poles and residues the differential cross sections are computed corresponding to the different Regge-type representations for the partial-wave amplitudes. In these representations the factor ξ is calculated from Eq. (A.4) using $\mu_0=a_0^{-1}$.

IV. RESULTS AND DISCUSSIONS

It is well known that the optical potential gives quite a satisfactory fit to experimental data for the elastic scattering of nucleons from nuclei. These fits are obtained by arbitrarily varying the optical-model parameters at each energy for the different nuclei. There is no consistency in the values of these parameters. However, these inconsistent optical-model parameters may be used to derive consistent and physically meaningful Regge-pole parameters. The main purpose of the present calculations is to investigate the validity of the complex angular-momentum approach to the optical model of elastic scattering of nucleons from spin-zero nuclei. We studied the elastic scattering of protons from C^{12} at the incident energies $E_p=4.613$ and 4.964 MeV. For these cases experimental phase shifts[11] are available. For the elastic scattering of neutrons from C^{12} and Ca^{40}, and of pro-

TABLE I. Poles of $a^{\pm}(\lambda, k)$ corresponding to the pole representation R4 for different elastic scattering processes.

E(lab) (MeV)	$\mathrm{Re}\lambda_1^+$	$\mathrm{Im}\lambda_1^+$	$\mathrm{Re}\lambda_1^-$	$\mathrm{Im}\lambda_1^-$	$\mathrm{Re}\lambda_2^+$	$\mathrm{Im}\lambda_2^+$	$\mathrm{Re}\lambda_2^-$	$\mathrm{Im}\lambda_2^-$	Scattering process
14.0	2.351	0.037	2.376	−0.025	3.5	0.121×10^{-2}	3.499	0.789×10^{-2}	$C^{12}(n,n)C^{12}$
2.06	0.437	−0.0089	0.437	−0.0089	2.211	−0.168	2.211	−0.168	$Ca^{40}(n,n)Ca^{40}$
3.29	0.425	0.04	0.437	−0.028	1.900	0.088	2.522	−0.521	
5.3	0.539	0.062	0.463	−0.0095	1.449	1.072	3.342	−0.163	
5.88	0.563	0.0013	0.457	−0.017	4.317	2.332	3.44	−0.146	
6.52	0.499	−0.0005	0.470	−0.0044	3.958	0.726	3.475	−0.171	
7.91	0.492	−0.018	0.477	−0.0049	3.69	−0.928	3.466	−0.169	
4.613	0.499	−0.0056	0.497	−0.0098	3.216	−0.287	2.169	0.172	$C^{12}(p,p)C^{12}$
4.964	0.500	−0.0048	0.498	−0.010	2.980	−0.253	2.283	0.171	
8.5	0.507	0.259	0.793	0.356	3.449	0.037	3.007	0.510	
11.85	1.272	0.702	1.432	0.488	3.502	0.039	3.512	0.134	
13.06	1.806	0.677	1.847	0.478	3.508	0.024	3.52	0.062	
14.0	2.292	0.440	2.207	0.230	3.508	0.011	3.531	0.039	
8.495	0.501	−0.0031	0.504	−0.0063	2.951	0.171	2.595	0.294	$O^{16}(p,p)O^{16}$
12.597	0.503	−0.0055	0.509	−0.013	3.315	0.233	3.147	0.693	
14.1	0.506	−0.0059	0.513	−0.015	3.818	0.544	3.409	1.326	

tons from C^{12} (at higher energies) and O^{16}, the complex optical potential[12-16] of the Woods-Saxon radial form containing a spin-orbit term is seen to reproduce the experimental data very well.

Using the experimental phase shifts or the optical-potential parameters as input, the exact partial-wave amplitudes are calculated. These are used for determining the Regge-pole parameters as explained in Sec. III. The Regge-pole and residue parameters corresponding to the representation $R4$ for the different elastic scattering processes at different energies are tabulated in Tables I and II. An examination of these parameters shows that at very low incident energies the spin-orbit interaction is hardly effective. For instance for $Ca^{40}(n,n)Ca^{40}$ scattering at $E_n = 2.06$ MeV, the positions of the poles λ_1^+ and λ_1^- coincide, and likewise for the case with λ_2^+ and λ_2^-. Similar results follow for the residue parameters also. As E increases these quantities become appreciably different.

Table I shows that for the scattering of the spin $\frac{1}{2}$-spin zero system, the Regge poles can occur in both quadrants of the right half of the λ plane in conformity with the proof given in Ref. 5. The pole

TABLE II. Residues of $a^{\pm}(\lambda, k)$ corresponding to the pole representation R4 for different elastic scattering processes.

E(lab) (MeV)	$\mathrm{Re}\beta_1^+$	$\mathrm{Im}\beta_1^+$	$\mathrm{Re}\beta_1^-$	$\mathrm{Im}\beta_1^-$	$\mathrm{Re}\beta_2^+$	$\mathrm{Im}\beta_2^+$	$\mathrm{Re}\beta_2^-$	$\mathrm{Im}\beta_2^-$	Scattering process
14.0	−0.088	0.176	−0.109	0.141	0.32×10^{-3}	-0.43×10^{-3}	2.9×10^{-3}	-0.46×10^{-3}	$C^{12}(n,n)C^{12}$
2.06	−0.031	0.055	−0.031	0.055	2.211	−0.168	2.211	−0.168	$Ca^{40}(n,n)Ca^{40}$
3.29	−0.020	0.071	−0.039	0.050	0.432	0.788	−0.453	−0.185	
5.3	0.161	−0.0017	−0.019	0.042	−15.74	−5.704	−0.054	−0.052	
5.88	0.016	−0.1217	−0.023	−0.047	−0.0021	−0.046	−0.026	−0.043	
6.52	−0.0009	0.0013	−0.0087	0.032	−0.0529	0.005	−0.015	−0.049	
7.91	−0.0205	0.0144	−0.0026	0.0255	0.0813	−0.014	−0.017	−0.051	
4.613	−0.012	0.002	−0.021	0.008	0.038	−0.0046	0.302	−0.249	$C^{12}(p,p)C^{12}$
4.964	−0.011	−0.0006	−0.021	0.0094	0.077	−0.023	0.268	−0.252	
8.5	0.311	0.457	4.324	−0.459	0.015	−0.0081	−0.137	−0.111	
11.85	12.31	39.82	0.0052	−0.0086	−7.945	10.5	−0.0026	−0.011	
13.06	4.737	2.461	0.0021	−0.0062	2.353	2.321	−0.0007	−0.0063	
14.0	0.535	0.069	0.0046	0.278	-0.502×10^{-4}	−0.0032	−0.0012	−0.0022	
8.495	−0.0040	0.0009	−0.0088	0.0014	0.196	−0.074	0.328	−0.184	$O^{16}(p,p)O^{16}$
12.597	−0.0057	0.0040	−0.011	0.0054	0.164	−0.106	−0.0041	−0.636	
14.1	−0.0051	-0.368×10^{-4}	−0.012	0.0022	0.010	−0.416	−2.796	−1.029	

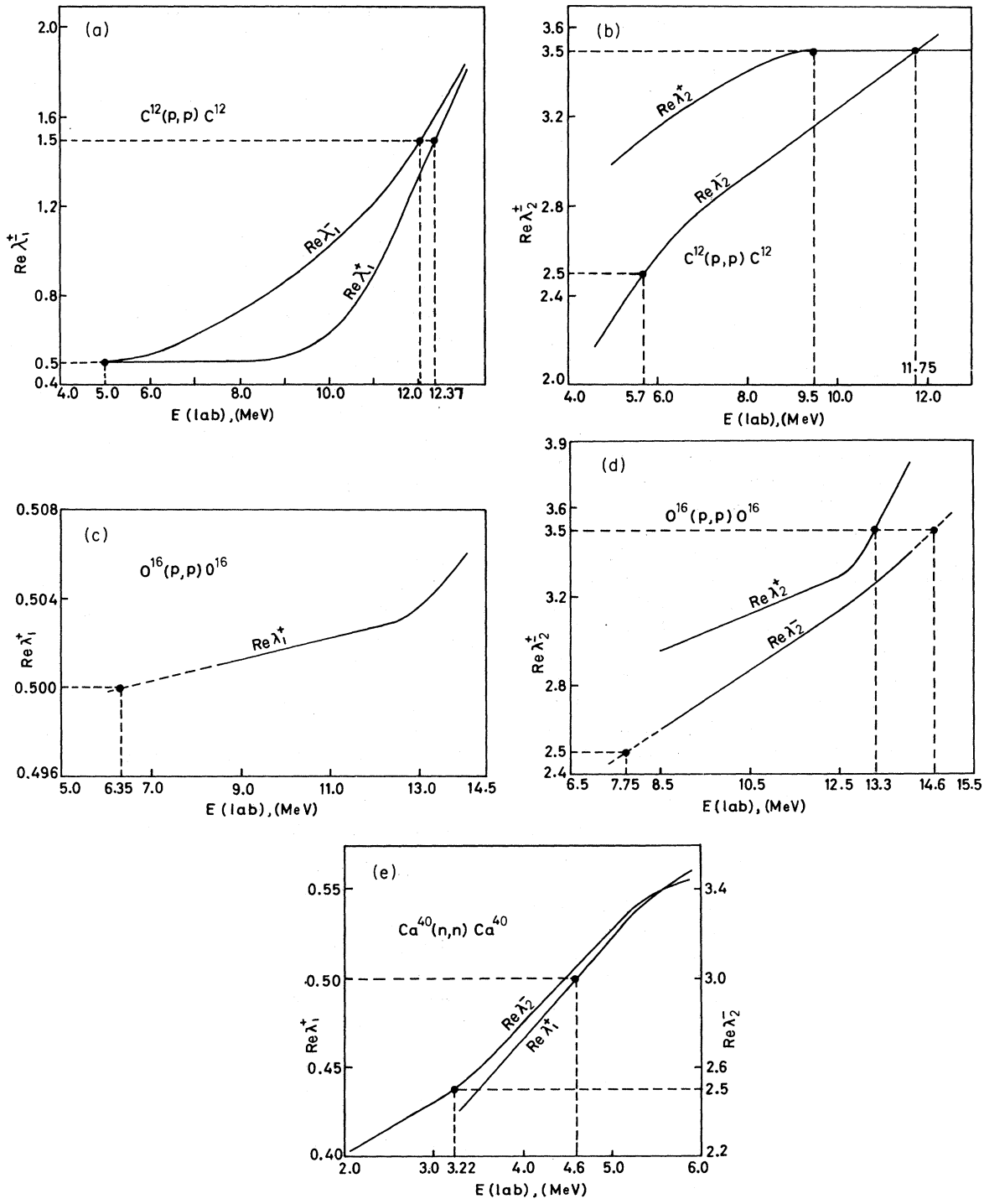

FIG. 1. (a) The real parts of $\lambda_1^\pm$ and (b) the real parts of $\lambda_2^\pm$ versus the incident energy in lab units for $C^{12}(p,p)C^{12}$. (c) The real parts of $\lambda_1^\pm$ and (d) the real parts of $\lambda_2^\pm$ versus the incident energy in lab units for $O^{16}(p,p)O^{16}$. (e) The real parts of $\lambda_1^\pm$ and λ_2^- versus the incident energy in lab units for $Ca^{40}(n,n)Ca^{40}$. Solid circles indicate resonances.

TABLE III. Levels in N^{13} obtained from the Regge trajectory for $C^{12}(p,p)C^{12}$ compared with experimental data.

Trajectory	E(lab) (MeV)	l_p	J^π	E_x (Calc) (MeV)	E_x (Expt) (MeV)
$\mathrm{Re}\lambda_1^+$ vs E	5.0	0	$\frac{1}{2}^+$	6.556	6.60
	12.37	1	$\frac{3}{2}^-$	13.36	13.5[a]
$\mathrm{Re}\lambda_1^-$ vs E	12.05	1	$\frac{1}{2}^-$	13.06	···
$\mathrm{Re}\lambda_2^+$ vs E	9.5	3	$\frac{7}{2}^-$	10.71	10.36
$\mathrm{Re}\lambda_2^-$ vs E	5.7	2	$\frac{3}{2}^+$	7.2	6.908
	11.75	3	$\frac{5}{2}^-$	12.78	12.08[a]

[a] Spin and parity not assigned.

parameters are more or less consistent in accordance with the general behavior of Regge trajectories connecting the physical state of the interacting system. The leading or resonating trajectories corresponding to $j = l \pm \frac{1}{2}$ in the case of $Ca^{40}(n,n)Ca^{40}$, $C^{12}(p,p)C^{12}$, and $O^{16}(p,p)O^{16}$ connect different resonances and possess the other essential features of Regge trajectories. Some of these trajectories, which indicate excited states in N^{13}, F^{17}, and Ca^{41} compound nuclei, are illustrated in Figs. 1(a)–1(e), and their level parameters are tabulated in Tables III, IV, and V, respectively. In order to draw a fairly smooth trajectory, the graphical method prescribed in Ref. 4 of assuming a polynomial dependence with respect to energy is followed.

In Fig. 1(a), $\mathrm{Re}\lambda_1^\pm$ (real parts of the poles $\lambda_1^\pm$) are plotted versus the incident laboratory energy E(lab) for the $C^{12}(p,p)C^{12}$ system. The trajectory $\mathrm{Re}\lambda_1^+$ indicates a $\frac{1}{2}^+$ resonance at E(lab) = 5.0 MeV, which is an excited level in N^{13} at 6.556 MeV. This corresponds to the $\frac{1}{2}^+$ level at $E = 5.05$ MeV (excitation energy $E_x = 6.6$ MeV) observed in $C^{12}(p,p)C^{12}$ elastic scattering studies.[17] The $\mathrm{Re}\lambda_1^+$ trajectory indicates another resonance at $E = 12.37$ MeV, which is the $\frac{3}{2}^-$ level of N^{13} at $E_x = 13.36$ MeV. This may correspond to the level[18] of N^{13} at $E_x = 13.5$ MeV whose spin and parity are not known. The $\mathrm{Re}\lambda_1^-$ trajectory passes through a resonance of $C^{12}(p,p)C^{12}$ at $E = 12.05$ MeV, giving indication of a $\frac{1}{2}^-$ level of N^{13} at 13.06 MeV. Figure 1(b) shows the trajectories $\mathrm{Re}\lambda_2^\pm$ plotted versus E(lab). The $\mathrm{Re}\lambda_2^+$ trajectory passes through a $\frac{7}{2}^-$ level (see Table III) of excitation energy 10.71 MeV. Experimental energy-level data[17,18] show that there is a $\frac{7}{2}^-$ level of N^{13} at 10.36 MeV. The $\mathrm{Re}\lambda_2^-$ trajectory is seen to pass through $\frac{3}{2}^+$ and $\frac{5}{2}^-$ levels of excitation energies 7.2 and 12.78 MeV, respectively. Energy-level data[18] show that there is a $\frac{3}{2}^+$ level of N^{13} at 7.42 MeV and an excited state at 12.08 MeV whose spin and parity are not specified.

TABLE IV. Levels in F^{17} obtained from the Regge trajectory for $O^{16}(p,p)O^{16}$ compared with experimental data.

Trajectory	E(lab) (MeV)	l_p	J^π	E_x (Calc) (MeV)	E_x (Expt) (MeV)
$\mathrm{Re}\lambda_1^+$ vs E	6.35	0	$\frac{1}{2}^+$	6.564	6.56
$\mathrm{Re}\lambda_2^+$ vs E	13.3	3	$\frac{7}{2}^-$	13.11	13.03[a]
$\mathrm{Re}\lambda_2^-$ vs E	7.75	2	$\frac{3}{2}^+$	7.29	7.44
	14.6	3	$\frac{5}{2}^-$	14.337	14.3[a]

[a] Spin and parity not assigned.

TABLE V. Levels in Ca^{41} obtained from the Regge trajectory for $Ca^{40}(n,n)Ca^{40}$.

Trajectory	E(MeV) (lab)	l_n	J^π	E_x (Calc) (MeV)	E_x(Expt) (MeV)
$\mathrm{Re}\lambda_1^+$ vs E	4.6	0	$\frac{1}{2}^+$	12.85	···
$\mathrm{Re}\lambda_2^-$ vs E	3.22	2	$\frac{3}{2}^+$	11.48	···

Figure 1(c) shows a plot of $\mathrm{Re}\lambda_1^+$ versus E(lab) for the $O^{16}(p,p)O^{16}$ system. This trajectory, on extrapolation to lower energies, passes through a resonance at $E = 6.35$ MeV, giving a $\frac{1}{2}^+$ level of F^{17} at 6.564 MeV. This obviously corresponds to the experimentally observed[18] $\frac{1}{2}^+$ level in F^{17} at 6.56 MeV (see Table IV). The $\mathrm{Re}\lambda_2^\pm$ trajectories are shown in Fig. 1(d). The $\mathrm{Re}\lambda_2^+$ trajectory indicates a $\frac{7}{2}^-$ level in F^{17} at 13.11-MeV excitation energy. Energy-level data[18] show that there is an excited state of F^{17} at 13.03 MeV with unassigned spin and parity. The $\mathrm{Re}\lambda_2^-$ trajectory passes through two levels at excitation energies 7.29 and 14.337 MeV of spin and parity $\frac{3}{2}^+$ and $\frac{5}{2}^-$, respectively. Experimentally[18] a $\frac{3}{2}^+$ level is observed at 7.44 MeV in F^{17} and another level at 14.3 MeV whose quantum numbers are not specified.

Figure 1(e) illustrates the $\mathrm{Re}\lambda_1^+$ and $\mathrm{Re}\lambda_2^-$ trajectories of the $Ca^{40}(n,n)Ca^{40}$ system. They indicate the presence of two levels in Ca^{41} at excitation energies 11.48 and 12.85 MeV of spin and parity $\frac{1}{2}^+$ and $\frac{3}{2}^+$, respectively. These do not correspond to any of the experimentally observed levels[19] in Ca^{41}, all of which have excitation energies less than 9 MeV.

The differential cross section for the elastic scattering of nucelons by spin-zero nuclei is given by

$$d\sigma/d\Omega = |A_1(k,\cos\theta)|^2 + |A_2(k,\cos\theta)|^2 .$$

The Regge-pole and residue parameters corres-

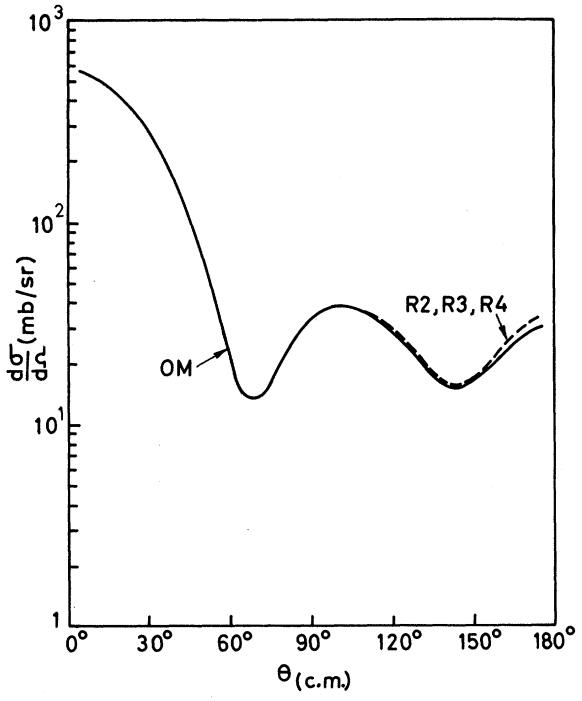

FIG. 2. $C^{12}(n,n)C^{12}$ angular distribution at $E_n = 14.0$ MeV. The solid line corresponds to the angular distribution obtained from the optical model and the dashed line indicates the same from λ-plane pole representation. The symbols designating the various representations are described in Sec. III.

ponding to the different Regge-type representations are used for calculating the partial-wave amplitudes $a^{\pm}(\lambda, k)$ and hence the differential cross sections. In all the cases considered, the representations R2, R3, and R4 for the partial-wave amplitudes yield equally good results.

In Fig. 2 the angular distributions for $C^{12}(n, n)C^{12}$ corresponding to the optical model (OM), and the representations R2, R3, and R4 at the incident lab energy $E_n = 14.0$ MeV are plotted. It is seen that R2, R3, and R4 are almost identical and give quantitative agreement with OM. The angular distributions for $Ca^{40}(n, n)Ca^{40}$ at the incident lab energies $E_n = 2.06$, 3.29, 5.3, 5.88, 6.52, and 7.91 MeV are illustrated in Figs. 3(a)–3(f). At $E_n = 2.06$ MeV the angular distributions corresponding to the representations R2, R3, and R4 exactly fit with that of OM. At $E_n = 3.29$ MeV, there is almost quantitative agreement between OM, R2, R3, and R4. As we proceed to higher energies, such as $E_n = 5.3$ and 5.88 MeV, we find that there is fair agreement between R2, R3, and R4 and OM. At still higher energies, for instance, $E_n = 6.52$ and 7.91 MeV, the fit is only qualitative for large angles, but there is almost quantitative agreement for small angles.

Figures 4(a) to 4(f) illustrate the angular distributions for $C^{12}(p,p)C^{12}$ at the incident energies $E_p = 4.613$, 4.964, 8.5, 11.85, 13.06, and 14.0 MeV. At $E_p = 4.613$ and 4.964 MeV the angular distributions corresponding to R2, R3, and R4 are compared with the exact curves obtained from experimental phase shifts.[11] At these two energies, it is seen that there is good agreement between R2, R3, R4, and the exact curve for backward angles, but only qualitative agreement exists for forward angles. Again at the higher incident energies $E_p = 8.5$ and 11.85 MeV there is only an over-all qualitative agreement between R2, R3, R4, and OM at all angles, and at $E_p = 13.06$ and 14.0 MeV there is almost quantitative agreement between the two curves at backward angles.

The angular distributions for $O^{16}(p,p)O^{16}$ at $E_p = 8.495$, 12.597, and 14.1 MeV are illustrated in Figs. 5(a)–5(c). In all these three cases it is seen that the fit between R2, R3, R4, and OM is only qualitative.

R3 represents the modified Regge-type representation without the damping factor, and R4 represents the same including the damping factor $[2\lambda/(\lambda + \lambda_n^{\pm})]$ in order to damp out the effects of the background integral. The equivalence of the results for R3 and R4 only shows that the damping factor is practically ineffective in these cases.

In the present work we have used a two-pole approximation for the partial-wave amplitudes. The fits to the experimental cross sections could perhaps be improved by using three or more poles. But then the simplicity of this approach would be lost. Since the damping factor of the background integral in the representation R4 is proved to be ineffective, it is necessary that we improve the representations for the partial-wave amplitudes such that the contribution from the background integral becomes negligible.

What we have achieved in the present investigations may be briefly stated as follows. Starting from a complex optical potential with an $\vec{l} \cdot \vec{S}$ force which has arbitrary parameters varying from energy to energy for the same nuclear scattering, we have obtained Regge trajectories which smoothly increase with energy connecting resonances of different l values. Some of these resonances correspond to actually observed ones, while others indicate the presence of new levels in N^{13}, F^{17}, and Ca^{41} compound nuclei. It may also be possible to predict the quantum numbers of existing nuclear levels of unassigned spin and parity. In addition, if the correct functional dependence of the residues with respect to energy were also known, then it would become possible to obtain the pole as well as the residue parameters at any intermediate energy in the range of the trajectories. These param-

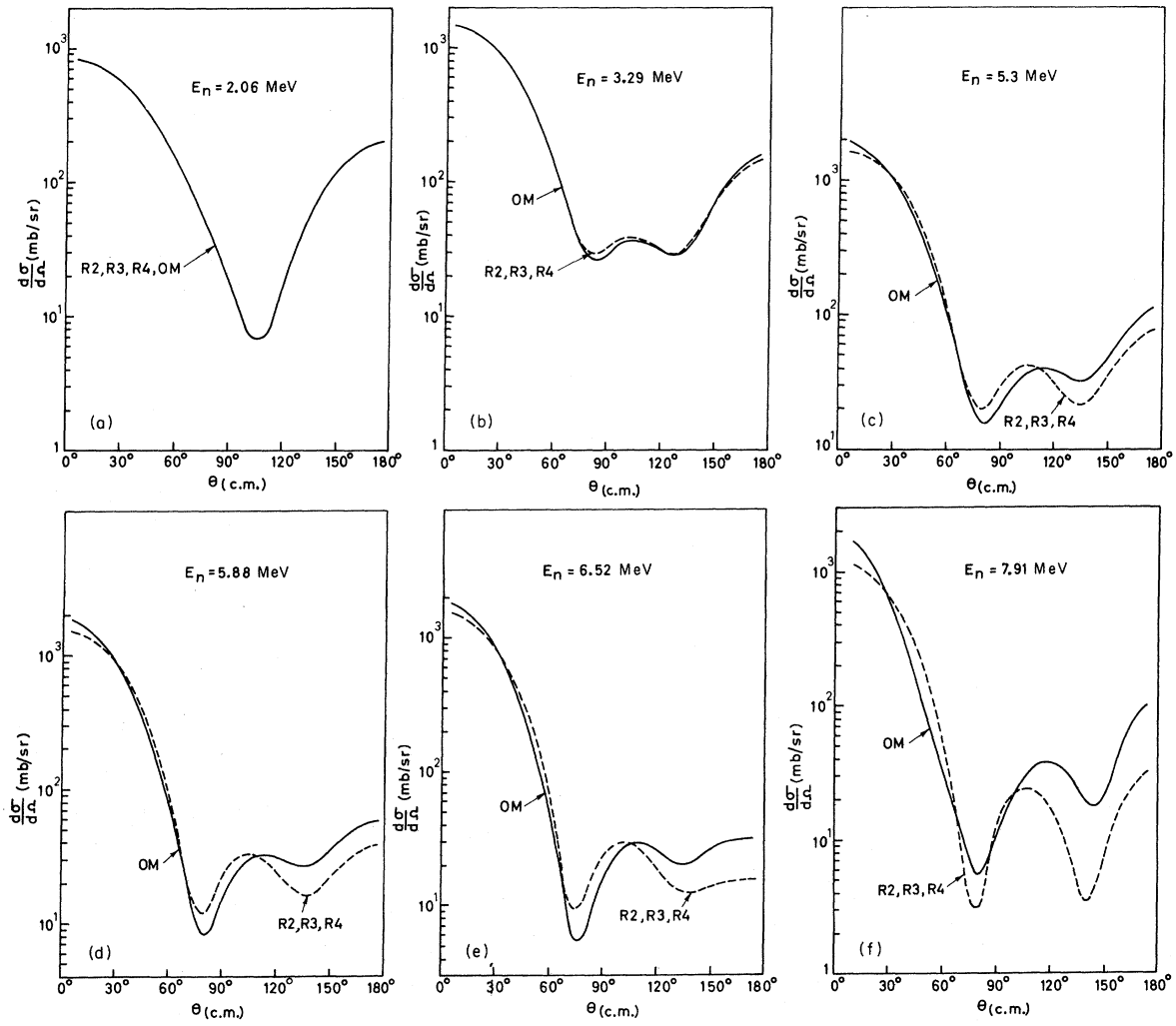

FIG. 3. $Ca^{40}(n,n)Ca^{40}$ angular distribution at different incident energies. Conventions similar to those of Fig. 2 are followed.

eters could be used for calculating the differential cross sections through appropriate Regge-type representation for the partial-wave amplitude. A knowledge of the optical-potential data at that energy is not necessary.

ACKNOWLEDGMENT

We are grateful for the computing facilities provided by the Tata Institute of Fundamental Research, Bombay. We are indebted to the Saha Institute of Nuclear Physics, Calcutta, where this work was first initiated, for the grant of Research Fellowships during the period.

APPENDIX. REGGE-TYPE REPRESENTATIONS FOR PARTIAL-WAVE AMPLITUDES WHEN A SPIN-ORBIT FORCE IS PRESENT

The elastic scattering of nucleons by a spin-zero target may be described in terms of the two amplitudes $A_1(k, z)$ and $A_2(k, z)$ which have the partial-wave expansions

$$A_1(k, z) = A_C(k, z) + \sum_l e^{2i\sigma_l}[(l+1)a^+(l, k) + la^-(l, k)]P_l(z) \quad \text{(A.1)}$$

and

$$A_2(k,z)=\sum_l e^{2i\sigma_l}[a^+(l,k)-a^-(l,k)]P_l^1(z), \tag{A.2}$$

where $A_C(k,z)$ is the Coulomb amplitude, $a^{\pm}(l,k)=[\bar{S}_l^{\pm}(k)-1]/2ik$, $\bar{S}_l^{\pm}(k)$ being the nuclear S matrix corresponding to the total angular momentum $j=l\pm\frac{1}{2}$ and $z=\cos\theta$.

Let us assume a Yukawa-type potential for the radial dependence of both the spin-independent and the spin-orbit interactions. It can be shown that for $k>0$, the asymptotic behavior of $\bar{S}^{\pm}(\lambda,k)$ [i.e., the analytically continued $\bar{S}_l^{\pm}(k)$ in the λ $(=l+\frac{1}{2})$ plane] is given by[20]

$$|\bar{S}^{\pm}(\lambda,k)-1|=O(|\lambda^{-1/2}e^{-\mathrm{Re}\lambda\xi}|), \tag{A.3}$$

where

$$\xi=\cosh^{-1}(1+\mu_0^2/2k^2), \tag{A.4}$$

and μ_0^{-1} is the highest value of the range appearing in a superposition of Yukawa potentials. The Legendre function has the asymptotic behavior[21]

$$P_{\lambda-\frac{1}{2}}(z)\underset{\substack{|\lambda|\to\infty\\ \mathrm{Re}\lambda\geq 0}}{\simeq}(2\pi)^{-1/2}l^{-1/2}(z^2-1)^{-1/4}e^X, \tag{A.5}$$

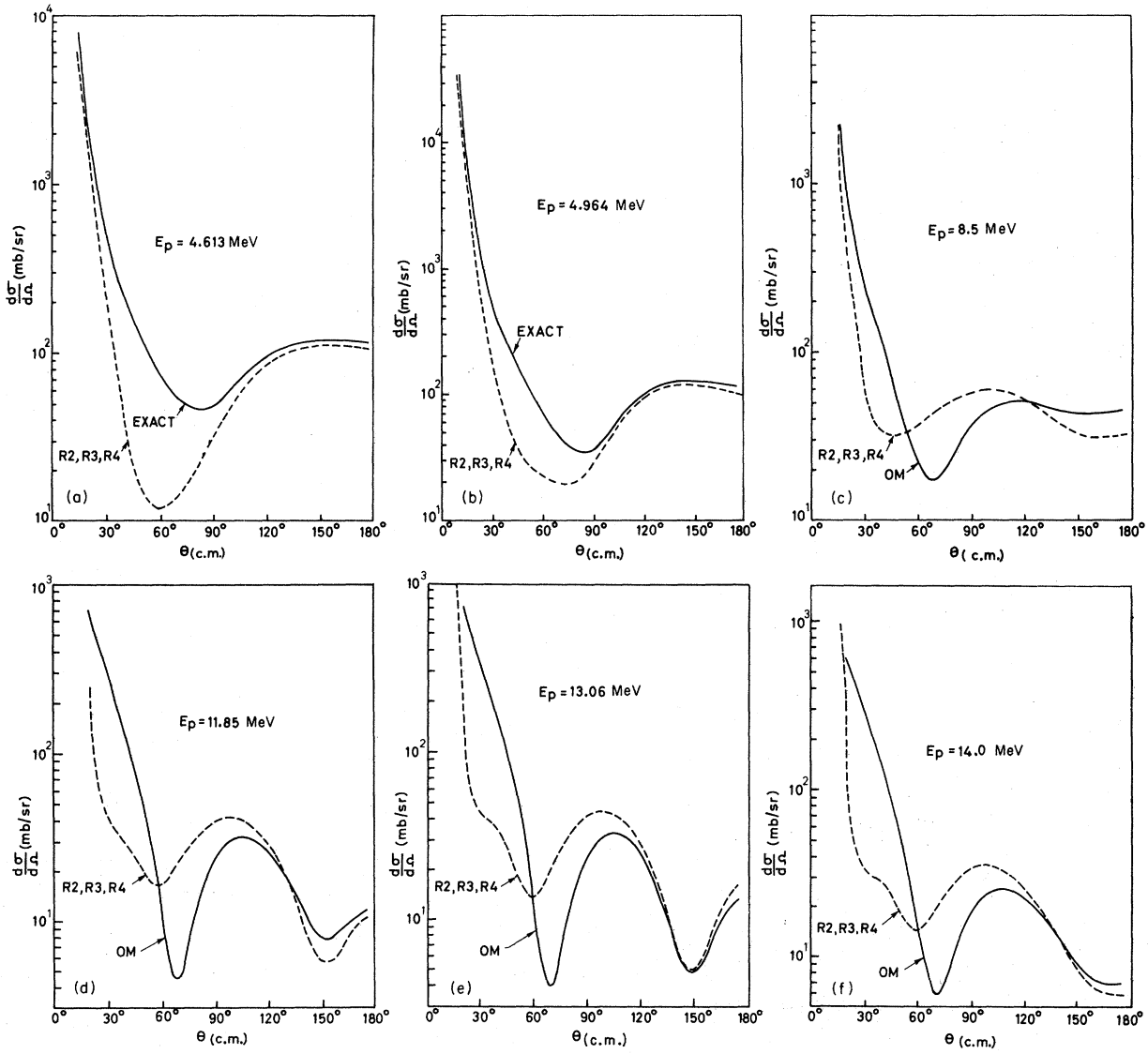

FIG. 4. $C^{12}(p,p)C^{12}$ angular distributions. The conventions of Figs. 2 and 3 are followed. In (a) and (b), the solid line corresponds to the results obtained from experimental phase shifts, and in (c)–(f) to the results from optical model.

where

$$X = 2|\mathrm{Im}\, l| \tan^{-1}[(1-z)/(1+z)]^{1/2},$$
$$= |\mathrm{Im}\, l|\,\theta \quad \text{for } z^2 < 1. \tag{A.6}$$

Therefore, the function

$$[(\lambda+\tfrac{1}{2})a^+(\lambda,k) + (\lambda-\tfrac{1}{2})a^-(\lambda,k)]P_{\lambda-\frac{1}{2}}(z)$$

has the asymptotic behavior $O(e^{-\mathrm{Re}\,\lambda\xi})$ in the right-half λ plane. Using this asymptotic property, one may perform the Sommerfeld-Watson (SW) transformation on the function

$$\bar{A}_1(k,z) = \sum_l [(l+1)a^+(l,k) + la^-(l,k)]\,P_l(z) \tag{A.7}$$

and obtain the representation

$$\bar{A}_1(k,z) = (2i)^{-1}\int_{-i\infty}^{i\infty} d\lambda' \,\frac{(\lambda'+\frac{1}{2})a^+(\lambda',k) + (\lambda'-\frac{1}{2})a^-(\lambda',k)}{\cos\pi\lambda'} P_{\lambda-\frac{1}{2}}(-z)$$
$$+\pi\left[\sum_{n=1}^{N^+}\beta_n^+ \frac{\lambda_n^+ + \frac{1}{2}}{\cos\pi\lambda_n^+} P_{\lambda_n^+ - \frac{1}{2}}(-z) + \sum_{n=1}^{N^-}\beta_n^- \frac{\lambda_n^- - \frac{1}{2}}{\cos\pi\lambda_n^-} P_{\lambda_n^- - \frac{1}{2}}(-z)\right]. \tag{A.8}$$

In the above expression $\lambda_n^\pm$ and $\beta_n^\pm$ denote the pole positions and residues of $a^\pm(\lambda,k)$, respectively, in the right half of the λ plane, and $N^\pm$ denotes the corresponding number of poles in this domain.

In (A.8), neglecting the background integral and splitting $\bar{A}_1$ into two terms

$$\bar{A}_1 = \bar{A}_1^+ + \bar{A}_1^-,$$

we have

$$\bar{A}_1^\pm(k,z) = \pi\sum_{n=1}^{N^\pm}\beta_n^\pm \frac{\lambda_n^\pm \pm \frac{1}{2}}{\cos\pi\lambda_n^\pm} P_{\lambda_n^\pm - \frac{1}{2}}(-z). \tag{A.9}$$

Taking the partial-wave projection of both sides of Eq. (A.9), using the formula

$$\tfrac{1}{2}\int_{-1}^{+1} dz\, P_l(z)P_\alpha(-z) = \frac{\sin\pi\alpha}{\pi(\alpha-l)(\alpha+l+1)}, \tag{A.10}$$

we obtain

$$\frac{\lambda \pm \frac{1}{2}}{2\lambda}\, a^\pm(\lambda,k) = \sum_{n=1}^{N^\pm}\beta_n^\pm \frac{\lambda_n^\pm \pm \frac{1}{2}}{\lambda^2 - (\lambda_n^\pm)^2}. \tag{A.11}$$

Similarly, using the asymptotic behavior[21] of $P_l^1(z)$ in l for $z^2 < 1$, one performs the SW transformation on the amplitude

$$\bar{A}_2(k,z) = \sum_l [a^+(l,k) - a^-(l,k)]P_l^1(z) \tag{A.12}$$

and obtains the Regge representation

$$\bar{A}_2(k,z) = (2i)^{-1}\int_{-i\infty}^{i\infty} d\lambda' \,\frac{a^+(\lambda,k) - a^-(\lambda,k)}{\cos\pi\lambda'} P^1_{\lambda'-\frac{1}{2}}(-z)$$
$$+\pi\left[\sum_{n=1}^{N^+}\beta_n^+ \frac{P^1_{\lambda_n^+ - \frac{1}{2}}(-z)}{\cos\pi\lambda_n^+} + \sum_{n=1}^{N^-}\beta_n^- \frac{P^1_{\lambda_n^- - \frac{1}{2}}(-z)}{\cos\pi\lambda_n^-}\right]. \tag{A.13}$$

In (A.13), neglecting the background integral and splitting $\bar{A}_2$ into two terms

$$\bar{A}_2 = \bar{A}_2^+ + \bar{A}_2^-,$$

we have

$$\bar{A}_2^\pm(k,z) = \pi\sum \beta_n^\pm \frac{P^1_{\lambda_n^\pm - \frac{1}{2}}(-z)}{\cos\pi\lambda_n^\pm}. \tag{A.14}$$

Taking the partial-wave projection of both sides of (A.14), using the formula[22]

$$\tfrac{1}{2}\int_{-1}^{+1} dz\, P_l^m(z)P_\alpha^m(-z) = \frac{\sin\pi\alpha\,\Gamma(\alpha+m+1)}{\pi\Gamma(\alpha-m+1)(\alpha-l)(\alpha+l+1)}, \tag{A.15}$$

we obtain

$$\frac{\lambda^2 - \frac{1}{4}}{2\lambda}\, a^\pm(\lambda,k) = \sum_{n=1}^{N^\pm}\beta_n^\pm \frac{(\lambda_n^\pm)^2 - \frac{1}{4}}{\lambda^2 - (\lambda_n^\pm)^2}. \tag{A.16}$$

Equations (A.11) and (A.16) represent Regge representations for $a^\pm(\lambda,k)$ obtained from the amplitudes $\bar{A}_1(k,z)$ and $\bar{A}_2(k,z)$, respectively. Since a correct representation for $a^\pm(\lambda,k)$ should have contributions from both the amplitudes $\bar{A}_1$ and $\bar{A}_2$, we combine the two forms given by Eqs. (A.11) and (A.16) and get the following Regge representation for $a^\pm(\lambda,k)$:

$$\frac{(\lambda \pm \frac{1}{2})^2}{2\lambda}\, a^\pm(\lambda,k) = \sum_{n=1}^{N^\pm}\beta_n^\pm \frac{(\lambda_n^\pm \pm \frac{1}{2})^2}{\lambda^2 - (\lambda_n^\pm)^2}. \tag{A.17}$$

Khuri Representation

The Khuri representation[23] is obtained by expressing a part of the background integral of the

Regge representation in terms of the poles in the right half of the λ plane.

The background integral I_1 of the Regge representation for $\bar{A}_1(k,z)$ is given by

$$I_1=(2i)^{-1}\int_{-i\infty}^{i\infty} d\lambda' \frac{[(\lambda'+\frac{1}{2})a^+(\lambda',k)+(\lambda'-\frac{1}{2})a^-(\lambda',k)]}{\cos\pi\lambda'} \times P_{\lambda'-\frac{1}{2}}(-z). \tag{A.18}$$

The Legendre function may be written as[24]

$$\frac{\pi P_{\lambda'-\frac{1}{2}}(-z)}{\cos\pi\lambda'}=\frac{1}{\sqrt{2}}\int_{-\infty}^{\infty}\frac{e^{\lambda' x}\,dx}{(\cosh x-z)^{1/2}}, \quad |\mathrm{Re}\lambda'|<\tfrac{1}{2}. \tag{A.19}$$

Integrating (A.19) partially twice, we obtain

$$\frac{\pi P_{\lambda'-\frac{1}{2}}(-z)}{\cos\pi\lambda'}=\frac{1}{2\sqrt{2}}\frac{1}{\lambda'^2}\int_{-\infty}^{\infty}e^{\lambda' x}g(x,z)dx, \quad |\mathrm{Re}\lambda'|<\tfrac{1}{2}, \tag{A.20}$$

where

$$g(x,z)=-\frac{d}{dx}\frac{\sinh x}{(\cosh x-z)^{3/2}}. \tag{A.21}$$

Substituting for $P_{\lambda'-\frac{1}{2}}(-z)$ from (A.20) in the background integral I_1, we have

$$I_1=\frac{1}{\sqrt{2}\,4\pi i}\int_{-i\infty}^{i\infty}\lambda'^{-2}[(\lambda'+\tfrac{1}{2})a^+(\lambda',k)+(\lambda'-\tfrac{1}{2})a^-(\lambda',k)] \times\int_{-\infty}^{\infty}e^{\lambda' x}g(x,z)dx\,d\lambda'. \tag{A.22}$$

If the nucleon-nuclear potential has a Woods-Saxon radial dependence, the asymptotic behavior of $a^{\pm}(\lambda,k)$ is given by

$$|a^{\pm}(\lambda,k)| \underset{\substack{|\lambda|\to\infty\\ \mathrm{Re}\,\lambda\geq 0}}{=} O(|\lambda^{1/2}e^{-\lambda\xi}|). \tag{A.23}$$

Therefore the function

$$\lambda^{-2}[(\lambda+\tfrac{1}{2})a^+(\lambda,k)+(\lambda-\tfrac{1}{2})a^-(\lambda,k)]$$

has the asymptotic behavior given by

$$O(|\lambda^{-1/2}e^{-\lambda\xi}|) \tag{A.24}$$

in the right half of the λ plane. Following Khuri's procedure we write

$$I_1=\frac{1}{\sqrt{2}\,4\pi i}\Big\{\int_{-i\infty}^{i\infty}\lambda'^{-2}[(\lambda'+\tfrac{1}{2})a^+(\lambda',k)+(\lambda'-\tfrac{1}{2})a^-(\lambda',k)]\int_{-\infty}^{\xi}e^{\lambda' x}g(x,z)dx\,d\lambda' +\int_{-i\infty}^{i\infty}\lambda'^{-2}[(\lambda'+\tfrac{1}{2})a^+(\lambda',k)+(\lambda'-\tfrac{1}{2})a^-(\lambda',k)]\int_{\xi}^{\infty}e^{\lambda' x}g(x,z)dx\,d\lambda'\Big\} \tag{A.25}$$

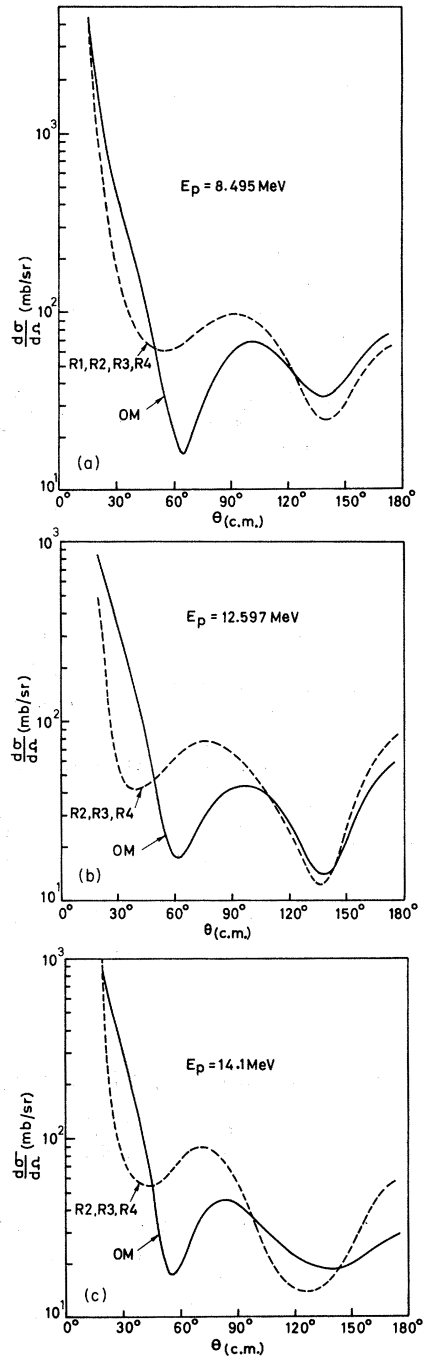

FIG. 5. $O^{16}(p,p)O^{16}$ angular distributions. The conventions of Figs. 2 and 3 are followed.

which gives, after interchanging the x and λ' integrations in the first term and then integrating over λ',

$$I_1 = \frac{-1}{2\sqrt{2}}\int_{-\infty}^{\xi} dx\, g(x,z)\left[\sum_{n=1}^{N^+}\frac{\lambda_n^+ + \frac{1}{2}}{(\lambda_n^+)^2}\beta_n^+ e^{\lambda_n^+ x} + \sum_{n=1}^{N^-}\frac{\lambda_n^- - \frac{1}{2}}{(\lambda_n^-)^2}\beta_n^- e^{\lambda_n^- x}\right]$$
$$+ \frac{1}{4\sqrt{2}\,\pi i}\int_{-i\infty}^{i\infty}\lambda'^{-2}\left[(\lambda'+\tfrac{1}{2})a^+(\lambda',k) + (\lambda'-\tfrac{1}{2})a^-(\lambda',k)\right]\int_{\xi}^{\infty} e^{\lambda' x} g(x,z)\,dx\,d\lambda'. \tag{A.26}$$

The Khuri representation for $\bar{A}_1(k,z)$ is obtained by including the first term of I_1 in the contribution of the pole terms of the Regge representation, while the second term represents the background integral I_1'. We therefore obtain

$$\bar{A}_1(k,z) = \pi\left[\sum_{n=1}^{N^+}\frac{\lambda_n^+ + \frac{1}{2}}{\cos\pi\lambda_n^+}\beta_n^+ P_{\lambda_n^+ - \frac{1}{2}}(-z) + \sum_{n=1}^{N^-}\frac{\lambda_n^- - \frac{1}{2}}{\cos\pi\lambda_n^-}\beta_n^- P_{\lambda_n^- - \frac{1}{2}}(-z)\right]$$
$$-\frac{1}{2\sqrt{2}}\int_{-\infty}^{\xi} dx\, g(x,z)\left[\sum_{n=1}^{N^+}\frac{\lambda_n^+ + \frac{1}{2}}{(\lambda_n^+)^2}\beta_n^+ e^{\lambda_n^+ x} + \sum_{n=1}^{N^-}\frac{\lambda_n^- - \frac{1}{2}}{(\lambda_n^-)^2}\beta_n^- e^{\lambda_n^- x}\right] + I_1'. \tag{A.27}$$

The Legendre function given by (A.20) has the inverse representation

$$g(x,z) = i\sqrt{2}\int_{-i\infty}^{i\infty} d\lambda'\,\lambda'^2 P_{\lambda'-\frac{1}{2}}(-z)\,\frac{e^{-\lambda' x}}{\cos\pi\lambda'}. \tag{A.28}$$

Neglecting I_1' in (A.27) and substituting (A.28) for $g(x,z)$, we obtain

$$\bar{A}_1(k,z) = \pi\left[\sum_{n=1}^{N^+}\frac{\lambda_n^+ + \frac{1}{2}}{\cos\pi\lambda_n^+}\beta_n^+ P_{\lambda_n^+ - \frac{1}{2}}(-z) + \sum_{n=1}^{N^-}\frac{\lambda_n^- - \frac{1}{2}}{\cos\pi\lambda_n^-}\beta_n^- P_{\lambda_n^- - \frac{1}{2}}(-z)\right]$$
$$-\frac{i}{2}\int_{-\infty}^{\xi} dx\left(\int_{-i\infty}^{i\infty}\lambda' P_{\lambda'-\frac{1}{2}}(-z)\,\frac{e^{-\lambda' x}}{\cos\pi\lambda'}\,d\lambda'\right)\left[\sum_{n=1}^{N^+}\frac{\lambda_n^+ + \frac{1}{2}}{(\lambda_n^+)^2}\beta_n^+ e^{\lambda_n^+ x} + \sum_{n=1}^{N^-}\frac{\lambda_n^- - \frac{1}{2}}{(\lambda_n^-)^2}\beta_n^- e^{\lambda_n^- x}\right]. \tag{A.29}$$

We first carry out the x integration which yields

$$-\frac{1}{2}i\int_{-i\infty}^{i\infty}\lambda'^2\,\frac{P_{\lambda'-\frac{1}{2}}(-z)}{\cos\pi\lambda'}\,d\lambda'\left[\sum_{n=1}^{N^+}\beta_n^+\,\frac{(\lambda_n^+ + \frac{1}{2})}{(\lambda_n^+)^2}\,\frac{e^{(\lambda_n^+ - \lambda)\xi}}{(\lambda_n^+ - \lambda)} + \sum_{n=1}^{N^-}\beta_n^-\,\frac{(\lambda_n^- - \frac{1}{2})}{(\lambda_n^-)^2}\,\frac{e^{(\lambda_n^- - \lambda)\xi}}{(\lambda_n^- - \lambda)}\right]. \tag{A.30}$$

The first integrand has poles at $\lambda = \lambda_n^+$ and poles at the zeros of $\cos\pi\lambda$ with residues $(-1)^{l+1}/\pi$. After carrying out the λ integration and substituting in (A.29), we have

$$\bar{A}_1(k,z) = \left[\sum_{n=1}^{N^+} P_{\lambda-\frac{1}{2}}(-z)\,\frac{\lambda^2}{(\lambda_n^+)^2}\,(\lambda_n^+ + \tfrac{1}{2})\beta_n^+\,\frac{e^{(\lambda_n^+ - \lambda)\xi}}{\lambda - \lambda_n^+} + \sum_{n=1}^{N^-} P_{\lambda-\frac{1}{2}}(-z)\,\frac{\lambda^2}{(\lambda_n^-)^2}\,(\lambda_n^- - \tfrac{1}{2})\beta_n^-\,\frac{e^{(\lambda_n^- - \lambda)\xi}}{\lambda - \lambda_n^-}\right]. \tag{A.31}$$

As before, splitting the amplitude $\bar{A}_1$ into two terms $\bar{A}_1^+$ and $\bar{A}_1^-$, we have

$$\bar{A}_1^{\pm}(k,z) = \sum_{n=1}^{N^{\pm}}\frac{\lambda^2}{(\lambda_n^{\pm})^2}(\lambda_n^{\pm} \pm \tfrac{1}{2})\beta_n^{\pm}\,\frac{e^{(\lambda_n^{\pm} - \lambda)\xi}}{\lambda - \lambda_n^{\pm}}\,P_{\lambda-\frac{1}{2}}(-z). \tag{A.32}$$

Taking the partial-wave projection of both sides of (A.32) gives

$$\frac{(\lambda \pm \frac{1}{2})}{\lambda^2}a^{\pm}(\lambda,k) = \sum_{n=1}^{N^{\pm}}\frac{\lambda_n^{\pm} \pm \frac{1}{2}}{(\lambda_n^{\pm})^2}\beta_n^{\pm}\,\frac{e^{(\lambda_n^{\pm} - \lambda)\xi}}{\lambda - \lambda_n^{\pm}}. \tag{A.33}$$

Following a similar procedure, we can deduce the Khuri representation for $\bar{A}_2(k,z)$ and the corresponding partial-wave amplitude.

Starting from the integral representation (A.19) for the Legendre function $P_{\lambda-\frac{1}{2}}(-z)$, we can easily find the integral representation for $P^1_{\lambda-\frac{1}{2}}(-z)$ as given by

$$P^1_{\lambda-\frac{1}{2}}(-z)=\frac{3}{4\sqrt{2}}\frac{(1-z^2)^{1/2}}{\pi}\frac{\cos\pi\lambda}{\lambda}\int_{-\infty}^{\infty}\frac{e^{\lambda x}\sinh x}{(\cosh x-z)^{5/2}}\,dx\,. \tag{A.34}$$

Substituting (A.34) in the background integral of the Regge representation (A.13) gives

$$I_2=\frac{3}{8\sqrt{2}}\frac{i}{\pi}(1-z^2)^{1/2}\int_{-i\infty}^{i\infty}\lambda^{-1}[a^+(\lambda,k)-a^-(\lambda,k)]\int_{-\infty}^{\infty}e^{\lambda x}\frac{\sinh x}{(\cosh x-z)^{5/2}}\,dx\,d\lambda\,. \tag{A.35}$$

The function $\lambda^{-1}[a^+(\lambda,k)-a^-(\lambda,k)]$ has the asymptotic behavior $O(|\lambda^{-1/2}e^{-\lambda\xi}|)$.

Now, proceeding as before, we obtain for the partial-wave amplitude

$$a^{\pm}(\lambda,k)=\sum_{n=1}^{N^{\pm}}\beta_n^+\frac{\lambda}{\lambda_n^+}\frac{e^{(\lambda_n^{\pm}-\lambda)\xi}}{\lambda-\lambda_n^{\pm}}\,. \tag{A.36}$$

Equations (A.33) and (A.36) are Khuri representations for $a^{\pm}(\lambda,k)$ obtained from the amplitudes $\bar{A}_1(k,z)$ and $\bar{A}_2(k,z)$, respectively. These two forms can be readily combined to yield the following Khuri representation for $a^{\pm}(\lambda,k)$:

$$\frac{1}{\lambda^2}a^{\pm}(\lambda,k)=\sum_{n=1}^{N^{\pm}}\beta_n^{\pm}\frac{1}{(\lambda_n^{\pm})^2}\frac{e^{(\lambda_n^{\pm}-\lambda)\xi}}{\lambda-\lambda_n^{\pm}}\,. \tag{A.37}$$

The general Khuri-type representation for the partial-wave amplitudes $a^{\pm}(\lambda,k)$ may be written as

$$\frac{1}{\lambda^2}a^{\pm}(\lambda,k)=\sum_{n=1}^{N^{\pm}}\beta_n^{\pm}\frac{1}{(\lambda_n^{\pm})^2}\frac{F(\lambda_n^{\pm},\lambda)}{\lambda-\lambda_n^{\pm}}\,, \tag{A.38}$$

where $F(\lambda,\lambda)=1$.

In the above equation, $F(\lambda_n^{\pm},\lambda)$ may be appropriately chosen to satisfy all the necessary physical features such as correct threshold behavior in k, asymptotic behavior in λ, correct Coulomb threshold behavior, and to have provision for damping the background-integral effects.

---

[1]T. Regge, Nuovo Cimento 14, 951 (1959); 18, 947 (1960).

[2]L. Rebolia and G. A. Viano, Nuovo Cimento 26, 1426 (1962).

[3]M. Carrassi and G. Passatore, Nuovo Cimento 32, 1337 (1964); M. Bertero, M. Carrassi, and G. Passatore, Nuovo Cimento 36, 854 (1965).

[4]R. Shanta and C. S. Shastry, Phys. Rev. 176, 1254 (1968).

[5]S. Mukherjee and C. S. Shastry, Nucl. Phys. A128, 256 (1969).

[6]S. Mukherjee, Phys. Rev. 160, 1546 (1967).

[7]J. V. Lepore, Phys. Rev. 79, 137 (1950).

[8]A. M. Lane and R. G. Thomas, Rev. Mod. Phys. 30, 257 (1958).

[9]P. B. Treacy, Nucl. Phys. A96, 145 (1967).

[10]V. De Alfaro and T. Regge, *Potential Scattering* (North-Holland Publishing Company, Amsterdam, The Netherlands, 1965).

[11]C. W. Reich, A. C. Philips, and J. L. Russel, Jr., Phys. Rev. 104, 143 (1956).

[12]A. J. Frasca, R. W. Finlay, R. D. Koshel, and R. L. Cassola, Phys. Rev. 144, 854 (1966).

[13]J. D. Reber and J. D. Brandenberger, Phys. Rev. 163, 1077 (1967).

[14]G. G. Shute, D. Robson, U. R. McKenna, and A. T. Berztiss, Nucl. Phys. 37, 535 (1962).

[15]J. S. Nodvik, C. B. Duke, and M. A. Melkanoff, Phys. Rev. 125, 975 (1962).

[16]G. Hardie, R. L. Dangle, and L. D. Oppliger, Phys. Rev. 129, 353 (1963); C. B. Duke, *ibid.* 129, 681 (1963).

[17]T. Lauritsen and F. Ajzenberg-Selove, Nucl. Phys. 11, 1 (1959).

[18]T. Lauritsen and F. Ajzenberg-Selove, *Nuclear Data Sheets*, compiled by K. Way *et al.* (Printing and Publishing Office, National Academy of Sciences – National Research Council, Washington, D. C.).

[19]P. M. Endt and C. Van der Leun, Nucl. Phys. A105, 1 (1967).

[20]S. Mukherjee and C. S. Shastry, Nucl. Phys. B3, 1 (1967).

[21]R. G. Newton, *Complex j-plane* (W. A. Benjamin, Inc.,

New York, 1964), p. 5, Eq. (2.4).
[22]*Higher Transcendental Functions*, Bateman Manuscript Project, edited by A. Erdélyi (McGraw-Hill Book Company, Inc., New York, 1953), Vol. 1, obtained from Eqs. (3.10.6), (3.12.7), and (3.12.21).
[23]N. N. Khuri, Phys. Rev. 130, 429 (1963).
[24]*Higher Transcendental Functions*, Bateman Manuscript Project, edited by A. Erdélyi (McGraw-Hill Book Company, Inc., New York, 1953), Vol. 1, p. 155, Eq. (1).

PHYSICAL REVIEW C VOLUME 2, NUMBER 4 OCTOBER 1970

Neutrons Emitted After Heavy-Ion Bombardment: Effects of Transfer Reactions on Particle Spectra*

William G. Simon and Stuart T. Ahrens
Department of Physics, The University of Wyoming, Laramie, Wyoming 82070
(Received 26 January 1970)

Measurements of neutron spectra from the reaction O^{16}(Ni,xn) and O^{16}(Ag,xn) with 160-MeV O^{16} ions and natural targets were made. Neutrons were detected at 15° intervals from 15 to 165°. Detection was accomplished with nuclear emulsions, using the internal-radiator method. The most striking feature of the spectra is the pronounced backward peaking in the c.m. system with ratios of $\sigma(180°)/\sigma(0°)$ as high as 2.0. We interpret this peaking to be caused by transfer reactions. Following the transfer reaction, a part of the incoming ion travels forward with its initial velocity, while the remaining partially fused system is traveling backward in the c.m. system. Evaporated particles from the partially fused system are thus backward peaked in the c.m. system. The charged-particle spectra for these same reactions, as measured by other investigators, are also analyzed in terms of transfer reactions. Qualitative agreement with some unusual aspects of the measured spectra is obtained.

I. INTRODUCTION

The use of heavy ions allows one to study compound-nuclear reactions at high excitations and high values of angular momentum. It is well known that protons or other light particles with energies as high as 100 MeV produce spectra that are interpretable in part by "cascade mechanisms," in which high-energy particles described as resulting from one or a few nucleon-nucleon collisions are observed. Eventually, the energy is shared by sufficient numbers of nucleons for the remainder of the deexcitation process to be described by the statistical model. If heavy ions are used, the initial energy is already shared by many nucleons, and it can be expected that cascade effects are small and that the entire deexcitation process is adequately described by the statistical model. It is therefore expected that heavy ions will allow a more simple and unambiguous test of the compound-statistical model at high excitation energies. Charged-particle emission is sensitive to the penetration of the Coulomb barrier, and uncertainties in the calculation of these effects make comparison with experiment difficult. A further effect of the Coulomb barrier is that only neutrons occur at low energies, where competition from nonstatistical processes is expected to be minimal. It appears, however, that it is a great advantage to have available data on all particles emitted copiously; this includes neutrons, protons, α particles and, to a lesser extent, deuterons.

Several measurements of the spectra of charged particles emitted in heavy-ion interactions have been reported.[1-4] Measurements of the total neutron yield from heavy-ion reactions have been given by Hubbard, Main, and Pyle,[5] and some recoil-technique experiments give neutron yields for reactions of the type (heavy-ion,xn).[6] Measurements of the spectra of neutrons have been made by Broek,[7] but detailed information on the angular distributions was not obtained.

In Sec. II, we give the results of the measurements of neutron spectra at 11 laboratory angles from the bombardment of natural nickel by 157-MeV O^{16} ions, and the bombardment of natural silver by 160-MeV O^{16} ions. The results show a backward peaking in the c.m. system, which we interpret in Sec. III to be a result of the transfer of part of the incoming ion to the target nucleus and subsequent evaporation from the resulting excited nucleus, which moves backward in the c.m. system.